Wannier Exciton in an Electric Field. I. Optical Absorption by Bound and Continuum States*

Daniel F. Blossey†
Physics Department, University of Illinois, Urbana, Illinois 61801
(Received 27 May 1970)

A comprehensive study of electric field effects on optical absorption by Wannier excitons is presented, showing field effects on both bound and continuum states. The calculations and results have been simplified by defining appropriate dimensionless parameters such that the eigenvalues are independent of field when expressed in terms of these parameters. A general normalization procedure for wave functions with continuous eigenvalues is outlined. The effect of the electron-hole interaction on the electric-field-induced oscillations is demonstrated, with the result that the electron-hole interaction enhances these oscillations near an M_0-type edge (positive effective masses) and quenches these oscillations near an M_3-type edge (negative effective masses). This effect would inhibit the observation of M_3-type edges in electroreflectance.

I. INTRODUCTION

The hydrogen atom in an electric field is perhaps the simplest quantum-mechanical problem for which there is no known analytic solution. The solution to this problem has applications in several areas, such as, field-controlled photogeneration of carriers in solids, trap-controlled mobilities, field ionization, and any problem which deals with a bound charge under the influence of an electric field. The problem that will be dealt with in detail here is the effect of an electric field on optical absorption by Wannier excitons. The Wannier exciton is an electron-hole pair created by photoexcitation of a crystalline solid.[1-4] This type of exciton is a hydrogenic atom typified by the effective masses of the electron and hole and by the dielectric constant of the solid. This model for the exciton is applicable to crystals which can generate charge carriers upon exposure to light, i.e., photoconductors. Also, from the formalism of the theory, it is required that the effective size of the excitation cover several unit cells of the crystal. The size of the excitation is related to how much an electron is shared among the various lattice sites. For covalently bonded crystals, the electron is shared equally among many sites and, consequently, the excitation covers many sites, but, for ionic, molecular, and rare gas solids, the electronic motion is much more restricted and the excitations are thereby more localized. These localized excitations are generally called Frenkel excitons.[5-9] Thus, the Wannier theory for excitons is primarily applicable to semiconductor crystals,[10] particularly from group IV of the Periodic Table; but many of the more qualitative results of this theory are applicable to noncovalently bonded crystals.[9]

By use of the effective-mass approximation, the Wannier exciton is equivalent to the hydrogen atom differing only in the values of the effective masses of the electron and hole and the dielectric constant of the medium.[2] The bound states of the electron-hole pair occur in the forbidden gap of semiconductors and insulators at energies given by

$$E_n = E_g - Rn^{-2}, \tag{1}$$

where E_g is the energy gap and R is the effective Rydberg energy. The intensities of the absorption lines for these bound levels are proportional to n^{-3}. These lines blend into a quasicontinuum for energies very near but just below the gap energy and then become a true continuum above the gap. The effective Rydberg R is given by

$$R = \mu e^4/2\hbar^2\epsilon^2 = (\mu/m)\epsilon^{-2} \times 13.6 \text{ eV}, \tag{2}$$

where μ is the reduced mass of the electron-hole pair, m is the electronic mass, and ϵ is the static dielectric constant of the solid. The radius (effective Bohr radius) of the exciton is given by

$$a = \hbar^2\epsilon/\mu e^2 = (\mu/m)^{-1}\epsilon \times 5.29\times10^{-9} \text{ cm}. \tag{3}$$

Thus, we see that a small effective mass (highly mobile carriers) and a large dielectric constant both combine to give large radii for the excitons, which is one of the criteria for validity of the Wannier theory. The electric field which is capable of ionizing the exciton must provide at least a potential drop of $1R$ across the effective Bohr radius, i.e., the ionization field $\mathcal{E}_I$ is defined as

$$\mathcal{E}_I = R/ea = (\mu/m)^2\epsilon^{-3} \times 2.59\times10^9 \text{ V/cm}. \tag{4}$$

In Table I, there is a listing of energy gaps, binding energies, and ionization fields for various semiconductors and insulators calculated from tabulated values of effective masses and dielectric constants[11-15]; the crystals are ordered by increasing value of energy gap.

There are very few published calculations on electric field effects on the hydrogenic atom. For calculation of Stark shifts and splittings,[16-19]

TABLE I. Energy gaps, exciton binding energies (exciton associated with highest energy split-off valence band), and ionization fields for various semiconductors and insulators.

Crystal	E_g (eV)	R (meV)	$\mathcal{E}_I$ (10^3 V/cm)
InSb	0.2357	0.5	0.08
InAs	0.360	1.8	0.70
Ge	0.800	1.4	0.55
GaSb	0.813	1.8	1.00
InP	1.29	6.5	7.8
GaAs	1.41	5.1	5.7
AlSb	1.6	7.5	12
CdTe	1.606	10.0	31
CdSe	1.8415	15.7	60
ZnTe	2.301	13.0	47
PbI_2	2.55	73.0	460
CdS	2.5831	29.4	140
ZnSe	2.818	19.0	75
ZnS	3.9115	40.1	200

perturbation methods are appropriate if $\mathcal{E}/\mathcal{E}_I \ll 1$. But for electric fields on the order of or larger than $\mathcal{E}_I$, the electric field dominates the Coulomb potential and a nonperturbative solution is needed. The first nonperturbative approach was proposed by Duke and Alferieff[20] in which they reduced the electric field plus Coulomb potentials to the analytically solvable model of only the Coulomb potential inside a given radius and only the electric field potential outside the given radius. This model is adequate in the high-field limit but fails to predict correct Stark shifts in the low-field limit. To improve on the results of Duke's model, numerical integrations of the hydrogenic Schrödinger equation have been performed by Ralph, [21] Dow and Redfield, [22] and the author. [23,24] Ralph[21] calculated the shifts and broadenings of the 1s hydrogenic level, and Dow and Redfield[22] demonstrated the electric field dependence of the excitonic absorption tail in the band gap and compared this with Urbach's rule. [25] Enderlein[26] used a Green's-function approach to solve the problem, but one of his assumptions made his results only valid in the limit $\mathcal{E}/\mathcal{E}_I \gg 1$. [27,28] Excitonic electroabsorption curves and measurable parameters will be displayed in a subsequent paper[29] as functions of electric field and temperature (broadening). The theory of optical absorption by Wannier excitons is briefly reviewed in Sec. II. The electric field effects on both bound and continuum exciton states are demonstrated in Sec. III. In Sec. III, it is shown that the parabolic coordinate eigenstates give both resonant peaks below the edge and electric-field-induced oscillations in the continuum, each oscillation being due to a different eigenstate. The calculation of WKB eigenvalues, which were within 1% of the actual eigenvalues, is presented in the Appendix. Extensive electroabsorption reviews may be found elsewhere.[30] Several useful excitonic electro-absorption parameters may be found in Table II.

II. WANNIER EXCITON THEORY

A. Effective-Mass Equation

From the band theoretical point of view, the absorption of light by a crystal is accomplished by creation of an electron-hole pair. The ground state of the crystal is assumed to be the state in which the valence band is completely filled and the conduction band is completely empty. The electron and hole in the final or excited state may interact via the Coulomb potential. This electron-hole interaction breaks the translational symmetry of the crystalline potential and mixes the Bloch waves. The excited state of the crystal may be approximated by a linear combination of Bloch electron and hole wave functions as follows

$$\Psi^{n,\vec{K}}(\vec{r}_e,\vec{r}_h)=\sum_{c,\vec{k}_e}\sum_{v,\vec{k}_h}A^{n,\vec{K}}_{c,v}(\vec{k}_e,\vec{k}_h)\psi_{c,\vec{k}_e}(\vec{r}_e)\psi_{v,-\vec{k}_h}(\vec{r}_h), \tag{5}$$

where n and $\vec{K}\equiv\vec{k}_e+\vec{k}_h$ are used to label the excited state, and $\psi_{c,\vec{k}_e}$ and $\psi_{v,-\vec{k}_h}$ are the electron and hole Bloch wave functions. The notation used here is consistent with that of Dimmock. [10] The energy difference E between the excited state $\Psi^{n,\vec{K}}$ and ground state Ψ_0 of the crystal may be determined from the following set of equations:

$$\begin{aligned}&[E_c(\vec{k}_e)-E_v(\vec{k}_h)-E]\,A^{n,\vec{K}}_{c,v}(\vec{k}_e,\vec{k}_h)\\&\quad+\sum_{c',\vec{k}'_e}\sum_{v',\vec{k}'_h}\langle c\vec{k}_e:v\vec{k}_h\,|\,V(\vec{r}_e-\vec{r}_h)\,|\,c'\vec{k}'_e:v'\vec{k}'_h\rangle\\&\quad\times A^{n,\vec{K}}_{c',v'}(\vec{k}'_e,\vec{k}'_h)=0\,,\end{aligned} \tag{6}$$

where $E_c(\vec{k}_e)$ and $E_v(\vec{k}_h)$ define the energy bands for the conduction- and valence-band states and $V(\vec{r}_e-\vec{r}_h)$ is any potential which causes mixing of the Bloch waves; in our case, the Coulomb potential is screened by a medium with dielectric constant

TABLE II. Definitions.

Quantity	Symbol	Definition	Units
Effective Ry	R	$\mu e^4/2\hbar^2\epsilon^2$	eV
Effective Bohr radius	a	$\hbar^2\epsilon/\mu e^2$	cm
Ionization field	$\mathcal{E}_I$	R/ea	V/cm
Reduced mass of electron-hole pair	μ	$m_e m_h/(m_e+m_h)$	g
Electro-optical energy	$\hbar\theta$	$(\mathcal{E}/\mathcal{E}_I)^{2/3}R$ $=(\hbar^2e^2\mathcal{E}^2/2\mu)^{1/3}$	eV
Broadening parameter	Γ	$\sim kT$	eV

ϵ and an external electric field is applied, whereby the electron-hole pair sees the combined potential

$$V(\vec{r}) = -e^2/\epsilon r - e\vec{\mathcal{E}}\cdot\vec{r}\ , \tag{7}$$

where $\vec{r} = \vec{r}_e - \vec{r}_h$ and $\vec{\mathcal{E}}$ is the electric field. This potential is shown in Fig. 1 for zero and finite electric field. The major effect of the electric field is to lower the lip of the potential well which causes the bound levels to be mixed and broadened into a continuum. A secondary effect of the electric field is a slight widening of the Coulomb well, which causes a shift of the 1s level to lower energies, which in turn produces the well-known phenomena of the second-order Stark shift.

As an aside, it should be noted that the Coulomb potential is not quite an accurate representation of the electron-hole "interaction." This is due to the fact that the electron and hole are not truly point particles but, in effect, have the dimensions of a unit cell of the crystal. This means that if the electron and hole are located in the same unit cell their charge clouds are overlapping and the potential well has a bottom on it instead of singular point at $r = 0$.[31] Using the Coulomb potential as being the electron-hole interaction causes overestimation of the binding energy of the lowest bound exciton level. In materials where more than two bound levels are observable, it has been shown that the 1s level deviates slightly from the $(E_n = E_g - Rn^{-2})$ rule.

The effective-mass equation of Dresselhaus[2] is obtained by introducing the Fourier transform of $A_{c,v}^{n,\vec{K}}(\vec{k}_e, \vec{k}_h)$ which is defined as

$$\Phi_{c,v}^{n,\vec{K}}(\vec{r}_e, \vec{r}_h) = \sum_{\vec{k}_e}\sum_{\vec{k}_h} e^{i\vec{k}_e\cdot\vec{r}_e} e^{i\vec{k}_h\cdot\vec{r}_h} A_{c,v}^{n,\vec{K}}(\vec{k}_e, \vec{k}_h)\ . \tag{8}$$

If we assume that $V(\vec{r})$ varies slowly over the distance of a unit cell and that the energy bands are nondegenerate, then $\Phi_{c,v}^{n,\vec{K}}(\vec{r}_e, \vec{r}_h)$ satisfies the differential equation

$$[E_c(i\nabla_e) - E_v(-i\nabla_h) + V(\vec{r}) - E]\,\Phi_{c,v}^{n,\vec{K}}(\vec{r}_e, \vec{r}_h) = 0\ . \tag{9}$$

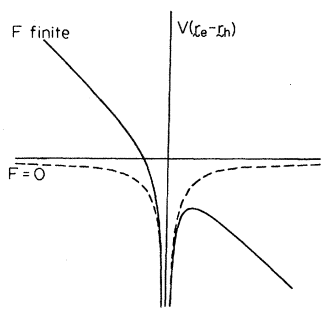

FIG. 1. Electron-hole interactions with and without externally applied electric field.

Using the effective-mass approximation and assuming that the bands are isotropic near the band edge gives

$$\left(-\frac{\hbar^2}{2\mu}\nabla^2 - V(\vec{r})\right)\phi_n(\vec{r}) = \left(E_n - \frac{\hbar^2K^2}{2M}\right)\phi_n(\vec{r})\ , \tag{10}$$

where $E_n = E - E_g$, E_g is the energy gap at the band edge, and $\phi_n(\vec{r})$ is defined by the equation

$$\Phi_{c,v}^{n,\vec{K}}(\vec{r}_e, \vec{r}_h) = e^{i\vec{K}\cdot\vec{R}}\phi_n(\vec{r})\ . \tag{11}$$

Here $\vec{r}$ is the relative coordinate, $\vec{R}$ is the center-of-mass coordinate, μ is the reduced mass of the electron-hole pair, and M is the sum of the electron and hole masses. Equation (10) is the equation that must be solved to determine the wave function for the Wannier exciton in an electric field, but before we seek a solution it is appropriate to determine the relationship between the optical absorption by Wannier excitons and $\phi_n(\vec{r})$.

B. Allowed and Forbidden Optical Transitions

If we include both bound and continuum exciton levels, then it may be stated that the entire absorption spectra is due to the formation of excitons. This is said to emphasize the point that the single-particle optical density of states is altered by the electron-hole interaction not only in the region directly below the energy gap but throughout the entire spectra. Thus we will be interested in calculating absorption by not only the bound exciton states but also the continuum exciton states.

The matrix element that determines the transition rate for optical transitions between the ground state Ψ_0 and the excited state $\Psi^{n,\vec{K}}$ is given by

$$M^{n,\vec{K}} = \langle\Psi^{n,\vec{K}}|(ie\hbar A/mc)e^{i\vec{q}\cdot\vec{r}}\hat{\epsilon}\cdot\nabla|\Psi_0\rangle\ , \tag{12}$$

where $\vec{A} = A\hat{\epsilon}e^{i\vec{q}\cdot\vec{r}-i\omega t}$ is the vector potential of the electromagnetic wave. Using $\Psi^{n,\vec{K}}$ from Eq. (5) and neglecting the momentum of the photon $\hbar\vec{q}$ relative to the crystal momentum $\hbar\vec{K}$, the matrix element $M^{n,\vec{K}}$ may be expressed as

$$M^{n,\vec{K}} = \sum_{\vec{k},c,v} A_{c,v}^{n,\vec{K}}(\vec{k}, -\vec{k})\left(\frac{ie\hbar A}{mc}\right)\delta_{\vec{K},0} \times\left\{\int_\Omega d\vec{r}\,u_{c,\vec{k}}^*\hat{\epsilon}\cdot\nabla u_{v,\vec{k}} + i\hat{\epsilon}\cdot\vec{k}\int_\Omega d\vec{r}\,u_{c,\vec{k}}^* u_{v,\vec{k}}\right\}\ , \tag{13}$$

where Ω is the volume of the unit cell of the crystal. The function $u_{\vec{k}}$ is defined in the normal manner as the part of the Bloch wave possessing the crystalline translational symmetry, i.e.,

$$\psi_{\vec{k}} = N^{-1/2}\,e^{i\vec{k}\cdot\vec{r}}\,u_{\vec{k}}\ .$$

Combining Eqs. (8) and (13), and assuming that the integrals in Eq. (13) are slowly varying functions of $\vec{k}$, one obtains the result[3]

$$M^{n,\vec{K}} = \sum_{c,v}\left(\frac{ie\hbar A}{mc}\right)\delta_{\vec{K},0} \times\left(\frac{i\hat{\epsilon}}{\hbar}\cdot\vec{P}_{cv}\,\phi_n(0) + U_{cv}\left|\hat{\epsilon}\cdot\nabla\phi_n\right|_{r=0}\right), \quad (14)$$

where $\vec{P}_{cv}$ and U_{cv} are defined by the integrals

$$\vec{P}_{cv} = (\hbar/i)\int_\Omega d\vec{r}\,u^*_{c,\vec{k}}\,\nabla u_{v,\vec{k}}\ , \quad (15a)$$

$$U_{cv} = \int_\Omega d\vec{r}\,u^*_{c,\vec{k}}\,u_{v,\vec{k}}\ . \quad (15b)$$

For allowed transitions, u_c and u_v are antisymmetric and $U_{cv}\simeq 0$; for forbidden transitions, u_c and u_v have the same point group symmetry and $P_{cv}\simeq 0$. The imaginary part of the dielectric constant is related to $M^{n,K}$ by the relation

$$\epsilon_2 = \frac{4\pi^2c^2}{\omega^2A^2}\sum_{\substack{\vec{K},n\\c,v}}|M^{n,K}|^2\delta(E-\hbar\omega). \quad (16)$$

Thus for allowed transitions, ϵ_2 is given by

$$\epsilon_2 = \frac{4\pi^2e^2}{m^2\omega^2}\sum_{\substack{c,v\\\vec{K},0}}\delta_{\vec{K},0}|\hat{\epsilon}\cdot\vec{P}_{cv}|^2|\phi_n(0)|^2\delta(E_g+E_n-\hbar\omega), \quad (17)$$

and forbidden transitions is given by

$$\epsilon_2 = \frac{4\pi^2e^2}{m^2\omega^2}\sum_{\substack{c,v\\\vec{K};n}}\delta_{\vec{K},0}|U_{cv}|^2\hbar^2|\hat{\epsilon}\cdot\nabla\phi_n|^2_{r=0} \times\delta(E_g+E_n-\hbar\omega). \quad (18)$$

The imaginary part of the dielectric constant is proportional to the absorption coefficient α, i.e., $\epsilon_2 = nc\alpha/\omega$ where n is the index of refraction. The imaginary part of the dielectric constant is also related to the reflectance R through a Kramers-Kronig transformation.

In addition to the direct transitions, there are less probable transitions between extrema in the conduction and valence bands known as indirect transitions. These transitions go through intermediate states in the excitation process and are usually phonon-assisted.[32-36] Because of the absorption and emission of phonons, the total wave vector $\vec{K}$ is no longer a conserved quantity, and the initial and final electron states do not have to be at the same $\vec{k}$ vector. Indirect transitions can be caused by any imperfection in the lattice such as impurities or defects, but phonons are generally considered to give the strongest effect. Because they are second-order effects, indirect transitions are only observed if the indirect gap is less than the direct gap. If we consider the simple band model near the band edges in which

$$E_c(\vec{k}) = E_g + (\hbar^2/2m_e)(\vec{k}-\vec{k}_c^{\,0})^2, \quad (19a)$$

$$E_v(\vec{k}) = (\hbar^2/2m_n)(\vec{k}-\vec{k}_v^{\,0})^2, \quad (19b)$$

and the extremal points $\vec{k}_c^{\,0}$ and $\vec{k}_v^{\,0}$ are not the same, then ϵ_2 becomes

$$\epsilon_2^{\rm ind} = \frac{4\pi^2e^2}{m^2\omega^2}\sum_{l(\pm)}\sum_{n,\vec{K}}|C_l^{\pm}|^2|\phi^{n,\vec{K}}(0)|^2\delta(\hbar\omega - E \pm \hbar\omega_l), \quad (20)$$

where $C_l^{\pm}$ includes interband and phonon-interaction matrix elements for phonon of energy $\hbar\omega_l$, and

$$E = E_g - E_n + E_{\rm c.m.}\ . \quad (21)$$

If there is a continuum of states, $\sum_n \to \int dE_n$ and

$$\sum_{\vec{K}} \to \frac{(2M^3)^{1/2}}{2\pi^2\hbar^3}\int_0^\infty E_{\rm c.m.}^{1/2}\,dE_{\rm c.m.}\ . \quad (22)$$

With these substitutions, Eq. (20) becomes

$$\epsilon_2^{\rm ind} = \frac{4\pi^2e^2}{m^2\omega^2}\sum_{l(\pm)}|C_l^{\pm}|^2\frac{(2M^3)^{1/2}}{2\pi^2\hbar^3} \times\int_{-\infty}^{E_0}dE'\,(E_0-E')^{1/2}|\phi_{E'}(0)|^2, \quad (23)$$

where

$$E_0 = \hbar\omega - E_g \pm \hbar\omega_l\ . \quad (24)$$

Thus if we know $\phi^2(0)$ as a function of energy, then $\epsilon_2^{\rm ind}$ may be calculated from Eq. (23). If $\phi^2(0)$ is proportional to the square root of energy, then ϵ_2 shows the energy squared dependence,

$$\epsilon_2^{\rm ind} \propto (\hbar\omega - E_g \pm \hbar\omega_l)^2. \quad (25)$$

The additonal integral over energy for indirect transitions tends to smooth out any structure that might be present in $\phi^2(0)$ and thereby makes the electric-field-induced structure in $\epsilon_2^{\rm ind}$ very subtle.

III. ELECTRIC FIELD EFFECTS

In Sec. II, it was shown that, for direct allowed transitions, the imaginary part of the dielectric constant ϵ_2 is proportional to a sum over amplitudes $|\phi_n(0)|^2$ where n denotes the hydrogenic state of energy E_n. In this section, a dimensionless density-of-states function $\phi^2(0)$ is defined which contains all electric field phenomena and is normalized such that it approaches the free-particle continuum limit $[(\hbar\omega - E_g)/R]^{1/2}$ for $(\hbar\omega - E_g) \gg R$, where E_g is the gap energy and R the exciton binding energy. The properly normalized $\phi^2(0)$ is defined as

$$\phi^2(0) = 4\pi^2a^3\sum_n|\phi_n(0)|^2\delta\left[\frac{(E_g+E_n-\hbar\omega)}{R}\right] \quad (26)$$

where a is the exciton radius and $\phi_n(\vec{r})$ satisfies Eq. (10) with $\vec{K}=0$. For $\mathcal{S}=0$, the amplitudes $|\phi_n(0)|^2$ are equal to $(\pi a^3)^{-1}$ for s-like hydrogenic states and zero for any other, whereby

$$\phi^2(0) = 4\pi\sum_{n=1}^{\infty}n^{-3}\,\delta\left[\frac{(\hbar\omega - E_g + R_n^{-2})}{R}\right], \quad \hbar\omega < E_g \quad (27a)$$

$$\phi^2(0) = \frac{2\pi}{1-\exp\{-2\pi[(\hbar\omega - E_g)/R]^{-1/2}\}}\,, \quad \hbar\omega > E_g$$

Equation (27b) is the continuum expression of Elliott[3] which approaches the limit $[(\hbar\omega - E_g)/R^{1/2}$ for $(\hbar\omega - E_g) \gg R$. Equations (27a) and (27b) both approach the limit 2π for $\hbar\omega = E_g$, (27a) as a quasi-continuum and (27b) as a continuum. It will be shown in the following how the electric field alters Eqs. (27). The density-of-states function $\phi^2(0)$ is related to the imaginary part of the dielectric constant ϵ_2 through Eq. (17), which may be rewritten as

$$\epsilon_2 = 4\epsilon \left| \frac{\hat{\epsilon}\cdot\vec{P}_{cv}}{m\omega a} \right|^2 \phi^2(0)\,, \tag{28}$$

where ϵ is the static dielectric constant, $\hat{\epsilon}$ is the unit polarization vector for the electromagnetic wave, a is the exciton radius, and it is assumed that $\vec{P}_{cv}$ is a slowly varying function of $\vec{k}$. If a dipole matrix element $\vec{\mu}_{cv}$ is defined as

$$\vec{\mu}_{cv} = (e/m\omega)\,\vec{P}_{cv}\,; \tag{29}$$

then for unpolarized radiation

$$\epsilon_2 = \tfrac{4}{3}\epsilon \left| \vec{\mu}_{cv}/ea \right|^2 \phi^2(0)\,. \tag{30}$$

Thus, in this form, it is evident that the exciton absorptive strength is proportional to the ratio squared of the interband transition dipole moment to the exciton dipole moment with $\phi^2(0)$ containing any electric-field-induced structure. In the following, we will only concern ourselves with effects near the direct gap where exciton effects are so predominant.

A. Separation of Effective-Mass Equation

The assumption of direct transitions requires that $\vec{K} = \vec{k}_e + \vec{k}_h = 0$. Knowing that only solutions with $\vec{K} = 0$ are needed, the differential equation for $\phi_n(\vec{r})$ reduces to

$$\left[-\left(\frac{\hbar}{2\mu}\right)\nabla^2 - \frac{e^2}{\epsilon r} - e\mathcal{E}z\right]\phi_n(\vec{r}) = E_n\phi_n(\vec{r})\,, \tag{31}$$

where the electric field $\mathcal{E}$ is taken to be in the z direction. This is the Schrödinger equation for the hydrogenic atom in an electric field, with μ being the reduced mass of the electron-hole pair and ϵ the static dielectric constant of the crystal. As mentioned previously, the externally applied electric field in the crystal can be large enough so that it is not simply a perturbation on the Coulomb field. Fields on the order of 10^5 V/cm are sufficient to ionize excitons in most crystals which means that the electric field can be comparable if not stronger than the Coulomb field. Thus, in the following, we will not treat the electric field as simply being a perturbation on the Coulomb field but will treat both equally. Our approach is to solve Eq. (31) by separation into parabolic coordinates followed by a numerical integration of the resulting differential equations.

Because of the linearity of the electric field potential, Eq. (31) is separable in parabolic coordinates. Parabolic coordinates, in fact, are useful in the treatment of all kinds of problems in which a particular direction in space is distinguished by some external force.[19] The parabolic coordinates ζ, η, and ϕ are defined as

$$\zeta = r + z, \quad \eta = r - z, \quad \text{and } \phi = \tan^{-1}(y/x)\,. \tag{32}$$

The surfaces $\zeta = \text{const}$ and $\eta = \text{const}$ are paraboloids of revolution about the z axis having the origin as focus. The volume element is given by

$$d\vec{r} = \tfrac{1}{4}(\zeta + \eta)\,d\zeta\,d\eta\,d\phi\,, \tag{33}$$

and the Laplacian operator is defined as

$$\nabla^2 = \frac{4}{\zeta+\eta}\left[\frac{\partial}{\partial\zeta}\left(\zeta\frac{\partial}{\partial\zeta}\right) + \frac{\partial}{\partial\eta}\left(\eta\frac{\partial}{\partial\eta}\right)\right] + \frac{1}{\zeta\eta}\frac{\partial^2}{\partial\phi^2}\,. \tag{34}$$

Equation (21) may be separated by defining $\phi_n(\vec{r})$ as a product of parabolic coordinate functions,

$$\phi_n(\vec{r}) = A f_\nu(\eta) g_{\nu'}(\zeta) e^{\pm im\phi}\,, \quad \nu' = \nu + \mu e^2/\epsilon\hbar^2\,, \tag{35}$$

where A is a normalization constant and the functions f_ν and $g_{\nu'}$ satisfy the equations

$$\frac{1}{\eta}\frac{d}{d\eta}\left(\eta\frac{df_\nu}{d\eta}\right) + \left(-\frac{m^2}{4\eta^2} - \frac{\nu}{\eta} + \frac{\mu E_n}{2\hbar^2} - \frac{\mu e\mathcal{E}\eta}{4\hbar^2}\right) f_\nu(\eta) = 0\,, \tag{36a}$$

$$\frac{1}{\zeta}\frac{d}{d\zeta}\left(\zeta\frac{dg_{\nu'}}{d\zeta}\right) + \left(-\frac{m^2}{4\zeta^2} + \frac{\nu'}{\zeta} + \frac{\mu E_n}{2\hbar^2} + \frac{\mu e\mathcal{E}\zeta}{4\hbar^2}\right) g_{\nu'}(\zeta) = 0\,. \tag{36b}$$

At this point in the calculation, it is convenient to define dimensionless variables so that the calculated eigenvalues will not be directly dependent on the values of the electric field, reduced mass, and static dielectric constant, but will be dependent only on two dimensionless parameters containing these variables. The two dimensionless parameters of importance are a dimensionless energy β and a dimensionless field $\mathcal{E}/\mathcal{E}_I$. The dimensionless energy β is

$$\beta = E_n/\hbar\theta = (E - E_g)/\hbar\theta\,, \tag{37}$$

where $\hbar\theta$ is the electro-optical energy and is defined as

$$\hbar\theta = (\hbar^2 e^2 \mathcal{E}^2/2\mu)^{1/3}\,. \tag{38}$$

The separation constants, or eigenvalues, ν and ν' may be made dimensionless by defining new variables κ and κ' which are given by

$$\kappa = (4\hbar^2/\mu e\mathcal{E})^{1/3}\,\nu, \quad \kappa' = \kappa + 2(\mathcal{E}_I/\mathcal{E})^{1/3}\,, \tag{39}$$

where $\mathcal{E}_I$ is the ionization field for the ground state of the exciton and is defined by Eq. (3).

Let us also define a dimensionless distance x such that

$$x=(\mathcal{E}/\mathcal{E}_I)^{1/3}\ (\eta/2a),\quad x>0 \tag{40a}$$

$$x=(\mathcal{E}/\mathcal{E}_I)^{1/3}\ (\zeta/2a),\quad x<0 \tag{40b}$$

where a is the effective Bohr radius.

With these substitutions Eqs. (36a) and (36b) become

$$\frac{1}{x}\frac{d}{dx}\left(x\frac{d}{dx}\begin{bmatrix}f\\g\end{bmatrix}\right)+\left(-\frac{m^2}{4x^2}-\frac{1}{x}\begin{bmatrix}\kappa\\\kappa'\end{bmatrix}+\beta-x\right)\begin{bmatrix}f\\g\end{bmatrix}=0,\quad \begin{bmatrix}x>0\\x<0\end{bmatrix}. \tag{41}$$

Since in Eq. (17) we are only interested in calculating $\phi_n(\vec{r})=0$, it should be noted that the only nonzero values for $\phi_n(\vec{r})$ at $\vec{r}=0$ come from the $m=0$ terms, since

$$f(x)\sim(\pm x)^{|m|/2},\quad (x\to 0\pm). \tag{42}$$

Thus only the $m=0$ terms contribute to the exciton for direct allowed transitions. For $m=0$ Eq. (41) reduces to

$$\frac{1}{x}\frac{d}{dx}\left(x\frac{d}{dx}\begin{bmatrix}f\\g\end{bmatrix}+\left(-\frac{1}{x}\begin{bmatrix}\kappa\\\kappa'\end{bmatrix}+\beta-x\right)\begin{bmatrix}f\\g\end{bmatrix}=0,\quad \begin{bmatrix}x>0\\x<0\end{bmatrix} \tag{43}$$

where $\kappa'=\kappa+2\,(\mathcal{E}_I/\mathcal{E})^{1/3}$.

B. Eigenvalues and Wave-Function Normalization

The effective potential in Eq. (43) has singularities at the origin and at plus and minus infinity as shown in Fig. 2. Thus the solutions f and g for $x>0$ and $x<0$ respectively may be obtained by connecting the regular solution at infinity to the regular solution at the origin by either numerical integration or some other sort of interpolation scheme. The value of $g(x)$ at the origin may be determined by connecting the oscillatory asymptotic solution, given by

$$g_{\kappa',\beta}(x)\sim(-x+\beta)^{-3/4}\sin[\tfrac{2}{3}(-x+\beta)^{3/2}+\kappa'(-x+\beta)^{1/2}+\alpha], \tag{44}$$

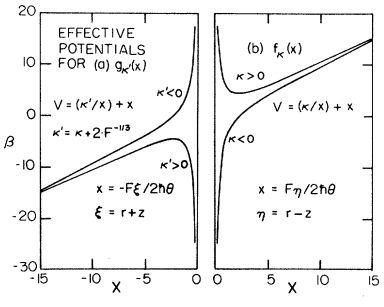

FIG. 2. Effective potentials for parabolic coordinate eigenfunctions (a) $g_{\kappa'}(x)$ and (b) $f_\kappa(x)$.

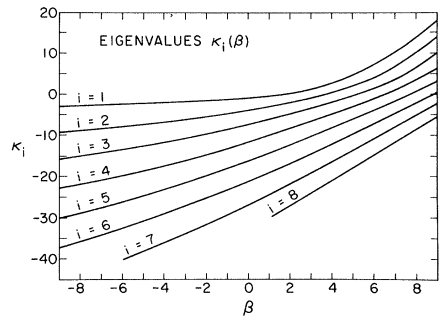

FIG. 3. Eigenvalues κ_i as functions of $\beta=(\mathcal{E}/\mathcal{E}_I)^{-2/3}\times[(E-E_g)/R]=(E-E_g)/\hbar\theta$ for eigenvalues $i=1-8$.

where α is an arbitrary phase angle, to a regular solution at the origin. Since the phase angle α is arbitrary, $g(0)$ is continuous function of κ' and β.

The asymptotic solution for $f(x)$ must fall off exponentially for $x\gg\beta$. Since only the exponentially decaying solution is allowed for large positive x, only certain values (eigenvalues) of κ will connect the regular solution at the origin to the asymptotic solution. The asymptotic solution for $f(x)$ is given by

$$f_{\kappa,\beta}(x)\sim(x-\beta)^{-3/4}\exp[-\tfrac{2}{3}(x-\beta)^{3/2}+\kappa(x-\beta)^{-1/2}]. \tag{45}$$

Connecting this solution to a regular solution at the origin determines a set of eigenvalues κ_i which are continuous functions of the dimensionless energy β.[24] A very good approximation to these eigenvalues κ_i may be obtained using the WKB approximation for calculating phase changes between classical turning points. The WKB eigenvalues κ_i^{WKB} are defined by the relationship (see the Appendix)

$$\int_{x_1}^{x_2}dx\left(-\frac{\kappa_i^{\mathrm{WKB}}}{x}+\beta-x\right)^{1/2}=(i-\tfrac{1}{2})\pi,\quad i=1,2,3,4,\ldots \tag{46}$$

where x_1 and x_2 are the classical turning points, i.e., the zeros of the integrand. It is interesting to note that the percent difference between κ_i^{WKB} and the actual κ_i was less than 1% so that the κ_i^{WKB} serve as a good starting point for an iteration procedure to find the κ_i. The solution of Eq. (46) is a hypergeometric function which may easily be calculated from various approximate series.[37] The κ_i approach the asymptotic limit $\kappa_i=-(2i-1)\,(-\beta)^{1/2}$ for large negative β. Since the eigenvalues are continuous functions of energy, the normalization of the wave function is quite different from normalization of wave functions which have discrete energy levels. The calculated eigenvalues $\kappa_i(\beta)$ are shown in Fig. 3.

Since $\phi_n(\vec{r})$ has continuous eigenvalues with respect to energy, it is necessary to normalize the integral of the wave function squared to a Dirac δ

function in energy instead of a Kronecker δ. The normalization expression is given by

$$\int d\vec{r}\ \phi^*_{E',\nu',m'}(\vec{r})\phi_{E,\nu,m}(\vec{r}) = \delta(E'-E)\delta_{\nu',\nu}\delta_{m',m}\,, \tag{47}$$

where E is the energy, ν is the separation constant, and m is the azimuthal quantum number. The wave function is a product of functions of the parabolic coordinates ζ, η, and ϕ

$$\phi_{E,\nu,m}(\vec{r}) = A f_{E,\nu,m}(\eta)\ g_{E,\nu,m}(\zeta) e^{\pm im\phi}. \tag{48}$$

The volume element $d\vec{r}$ and the Laplacian operator are given in Eqs. (33) and (34) in terms of parabolic coordinates. The $e^{\pm im\phi}$ part of the wave function leads directly to the $\delta_{m',m}$ normalization. The $f(\eta)$ function is bounded so that the integral of its modulus squared may be calculated by machine. The difficulty in evaluating the integral in Eq. (47) numerically is that the $g(\zeta)$ function is oscillatory and falls off slowly as is evident from its asymptotic solution in Eq. (44). Calculating the integral of its modulus squared is not possible by machine because this integral gives the Dirac δ function normalization which blows up for $E' = E$. Thus a different method for calculating the integral in Eq. (47) must be devised.

From Eq. (31), it is clear that

$$\int d\vec{r}\ [\phi'^*\nabla^2\phi - \phi\nabla^2\phi'^*] = \frac{2\mu}{\hbar^2}\ (E'-E)\int d\vec{r}\ \phi'^*\phi, \tag{49}$$

where the primed function ϕ' has eigenvalues E', ν', and m'. Combining Eqs. (31), (33), (48), and (49) gives the result

$$\begin{aligned}\frac{2\mu}{\hbar^2}\ (E'-E)\delta(E'-E)\delta_{\nu',\nu}&\\ = 2\pi A^2\left[\int_0^\infty d\zeta g'^* g\right]\left[\eta f'^*\frac{df}{d\eta} - \eta f\frac{df'^*}{d\eta}\right]_0^\infty&\\ + 2\pi A^2\left[\int_0^\infty d\eta f'^* f\right]\left[\zeta g'^*\frac{dg}{d\zeta} - \zeta g\frac{dg'^*}{d\zeta}\right]_0^\infty\,.&\end{aligned} \tag{50}$$

The first term on the right-hand side of Eq. (50) is zero since $f(\eta)$ is zero at infinity and η is, of course, zero at $\eta = 0$. Realizing also that the limit at $\zeta = 0$ of the second term on the right-hand side of Eq. (50) contributes nothing, we are left with

$$\frac{2\mu}{\hbar^2}\ (E'-E)\delta_{\nu',\nu} = 2\pi A^2\left(\int_0^\infty d\eta f'^* f\right) \times \lim_{\zeta\to\infty}\ \zeta\left(g'^*\frac{dg}{d\zeta} - g\frac{dg'^*}{d\zeta}\right). \tag{51}$$

Since the $f_{E\nu}$ form a discrete set at a given energy E, let f be normalized so that

$$\int_0^\infty d\eta f'^* f = \delta_{\nu',\nu}\ (\mathcal{E}_I/\mathcal{E})^{1/3} 2a \tag{52a}$$

or

$$\int_0^\infty dx f'^* f = \delta_{\kappa',\kappa}\,. \tag{52b}$$

The remaining part of Eq. (51) to evaluate is the asymptotic limit of the term containing $g(\zeta)$ and $g'(\zeta)$ which from Eq. (44) is

$$\zeta\left(g'^*\frac{dg}{d\zeta} - g\frac{dg'^*}{d\zeta}\right) \sim \sin\left[\left(\frac{\zeta}{2a}\right)^{1/2}\left(\frac{\mathcal{E}}{\mathcal{E}_I}\right)^{1/2} \times \left(\frac{E'-E}{R}\right)\right](\zeta\to\infty)\ \sim \pi(E'-E)\delta(E'-E). \tag{53}$$

Substituting Eqs. (52) and (53) into Eq. (51), and solving for A^2 we find that

$$A^2 = (4\pi^2 a^3 R)^{-1}. \tag{54}$$

Combining Eqs. (26), (48), and (52) gives the density-of-states function $\phi^2(0)$ in terms of $f^2_{\kappa_i}(0)$ and $g^2_{\kappa_i}(0)$ as

$$\phi^2(0) = \left(\frac{\mathcal{E}}{\mathcal{E}_I}\right)^{1/3}\ \sum_{i=1}^{\infty} f^2_{\kappa_i}(0)\,(0)\,, \tag{55}$$

where the δ function in energy has been eliminated by integrating over energy as implied from $\sum_n$. The sum over states n means a sum over the azimuthal quantum number m (only $m = 0$ terms are nonzero), a sum over the eigenvalues κ_i at each energy E, and an integral over energy since the electric field causes all states to form a continuum in energy. The normalization for $\phi^2(0)$ for $(\hbar\omega - E_g) \gg R$ holds for Eq. (55) as well as for Eq. (27) if it is also required that $(\hbar\omega - E_g) \gg \hbar\theta$. This aforementioned normalization requires that $\phi^2(0)$ approach $[(\hbar\omega - E_g)/R]^{1/2}$ far above the gap energy.

The values of $f^2_{\kappa_i}(0)$ are plotted as a function of dimensionless energy β in Fig. 4. These $f^2_{\kappa_i}(0)$ values are calculated by connecting the asymptotic solution for $f(x)$ given in Eq. (45) to a regular solution at the origin. For large negative β the $f^2_{\kappa_i}(0)$ functions all approach the limit $2(-\beta)^{1/2}$. The $f^2_{\kappa_i}(0)$ fall off quickly to zero for $\beta > \beta_i$, where

$$\beta_i = [\tfrac{3}{2}\pi(i - \tfrac{1}{2})]^{2/3}, \tag{56}$$

and the β_i are approximately the zeros of the $\kappa_i(\beta)$ as calculated in the Appendix. From Fig. 2(b) it is clear that the effective potential for $f(x)$ is repulsive near the origin for $\kappa > 0$ and attractive for $\kappa < 0$, thus causing the zeros of the $\kappa_i(\beta)$ to be cutoff points for the $f^2_{\kappa_i}(0)$.

Several curves of $g^2_{\kappa'}(0)$ as a function of κ' at constant β are plotted in Fig. 5. The eigenvalues κ_i' and κ_i are related by Eq. (39) and the κ_i' depend on the electric field strength. The resonant peaks in $g^2_{\kappa'}(0)$ increase in height and number for increasing negative β. The smaller the electric field the larger the value of $(\kappa_i' - \kappa_i)$ and the sharper the peaks in $g^2_{\kappa_i'}(0)$. Figure 6 shows, for $F = \mathcal{E}/\mathcal{E}_I = 0.008$, the

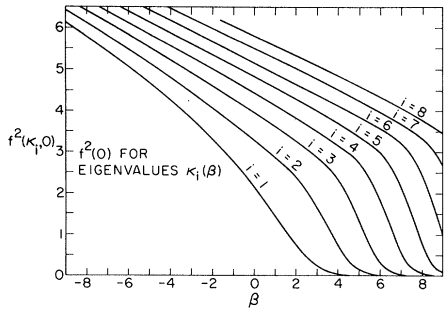

FIG. 4. Amplitudes $f^2_{\kappa_i}(0)$ as functions of β for eigenvalues $i=1$–8.

points of intersection of the κ_i' curves with the peak positions in $g^2_{\kappa'}(0)$. This figure shows schematically how the $n=2$ hydrogenic level is split by the electric field into two eigenstates of the parabolic coordinate Schrödinger equation. The $i=1$ parabolic coordinate eigenstate also contains the $n=1$ hydrogenic level whose peak position can be determined by continuing κ_i' to the point of intersection with the first resonant peak position of $g^2_{\kappa'}(0)$ at larger negative β. In fact, the $i=1$ state contains the lowest-energy split-off branch of each hydrogenic level n, the $i=2$ state contains the second branch of each level n starting with $n=2$, the $i=3$ state contains the third branch of each level n starting with $n=3$, etc. This result will be demonstrated in more detail in Sec. IV.

C. Bound States

In the limit of small electric fields ($\mathcal{E}/\mathcal{E}_I \ll 1$) the peaks in $\phi^2(0)$ represent the bound exciton states whose energies agree with perturbation theo-

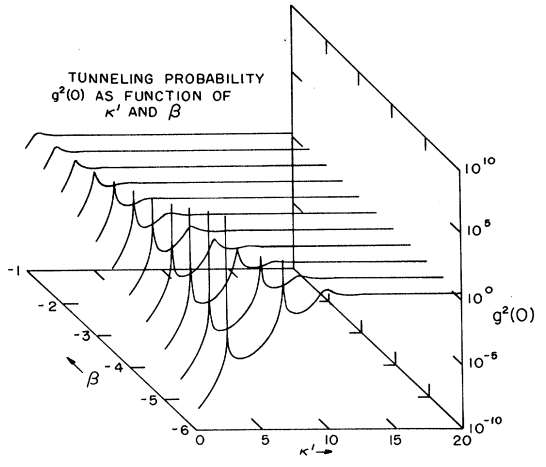

FIG. 5. Amplitudes $g^2_{\kappa'}(0)$ as functions of κ' and β. The specific values of κ' needed for a given field $\mathcal{E}$ are given by $\kappa_i' = \kappa_i + 2(\mathcal{E}/\mathcal{E}_I)^{-1/3}$.

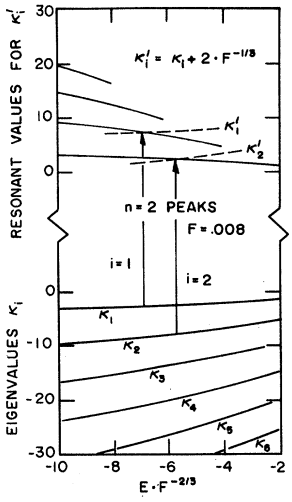

FIG. 6. Peak positions of $g^2_{\kappa_i}(0)$, eigenvalues κ_i, and values of κ_i' versus β for $F=\mathcal{E}/\mathcal{E}_I=0.008$. The drawing shows how the κ_i' intercept the peak positions in $g^2_{\kappa'}(0)$ which correspond to the bound hydrogenic levels. Here it is shown that the electric field causes a splitting in the $n=2$ level with the lower-energy branch corresponding to the $i=1$ eigenstate and the upper branch corresponding to the $i=2$ eigenstate.

ry (Stark effect). Each resonant state may be described by the parabolic coordinate quantum numbers (n,i,m) and these quantum numbers have a definite correspondence to the quantum numbers of the hydrogen atom (n,l,m), in fact, $n=n$, $m=m$.[19] Thus it would seem that the quantum number i replaces the orbital quantum number l and indeed this is the case. For example, for the case of $n=2$, $i=1$, $m=0$, and $\mathcal{E}=0$, the parabolic eigenfunction ϕ_{210} is related to the $R_{nl}Y_{lm}$ spherical coordinate eigenfunctions by the relation

$$\phi_{210} = (\sqrt{\tfrac{1}{2}})R_{20}Y_{00} + (\sqrt{\tfrac{1}{2}})R_{21}Y_{10}. \tag{57}$$

Thus the effect of using parabolic coordinates is to mix degenerate states along the direction of the field, in this case, and S and P_z states for the $n=2$ level. Application of a field in the z direction gives preference to the parabolic coordinates and mixes the spherical coordinate eigenstates. In general, the parabolic-coordinate eigenfunctions are given by (for $m=0$)

$$\phi_{ni0} = \frac{\exp[-(1/2n)(\xi+\eta)]}{n^2\pi^{1/2}(n-i)!\,(i-1)!\,L^0_{n-i}(\eta/n)}. \tag{58}$$

where $\xi = r+z$, $\eta = r-z$ and the $L^0_k(x)$ are the associated Laquerre functions, which are defined by a generating function as

$$(1-t)^{-1}\exp\left(\frac{-xt}{1-t}\right) = \sum_k L^0_k(x)\frac{t^k}{k!}. \tag{59}$$

Table III shows the ϕ_{ni0} for $n=1,2,3$ as functions of the spherical coordinate hydrogen atom eigenfunctions $R_{nl}Y_{lm}$.

The addition of the electric field then perturbs the states ϕ_{nim} and causes shifts in the energy of these states. To third order in electric field $\mathcal{E}$, the

energy of the various states (nim) is given by

$$E_{nim}/R = -1/n^2 - \tfrac{3}{2}(\mathcal{E}/\mathcal{E}_I)\, n(n-2i-m+1) - \tfrac{1}{32}(\mathcal{E}/\mathcal{E}_I)^2 n^4 [17n^2 - 3(n-2i-m+1)^2 - 9m^2 + 19] - \tfrac{3}{128}(\mathcal{E}/\mathcal{E}_I)^3 n^7 (n-2i-m+1) \times [23n^2 - (n-2i-m+1)^2 + 11m^2 + 39]. \quad (60)$$

As indicated before, these low-field eigenstates correspond to peaks in

$$\phi^2(0) = (\mathcal{E}/\mathcal{E}_I)^{1/3} \sum_t f^2_{\kappa_t}(0)\, g^2_{\kappa_t'}(0)$$

and that each peak is associated with a certain eigenvalue κ_t. Figure 5 shows that for $\kappa_t' > 0$, $\beta < 0$, resonant peaks can occur in $g^2_{\kappa_t'}(0)$ and the peak height increases with increasing negative β.

A few general features of the effect of an electric field can be seen by simply examining the effect of a uniform electric field on the Coulomb potential. The Coulomb potential with and without electric field was shown in Fig. 1. The major effect of the electric field is to lower the lip of the well and thereby change discrete bound states into continuum states. When the lip of the well moves below the energy of a bound level, then it takes no extra energy to separate the electron and hole and that level is said to be ionized. A secondary effect of the electric field is to slightly widen the well. This causes the ground exciton state to shift to a lower energy because, from the WKB point of view, a wave function with given quantum numbers must retain a certain phase shift between classical turning points. Thus if the well widens, the level must shift to a lower energy. These results will be seen in more detail in Sec. IV.

In the following, the function $\phi^2(0)$, which is proportional to ϵ_2 (the imaginary part of the dielectric constant) and α (the absorption coefficient), will be plotted as a function of energy for several values of $\mathcal{E}/\mathcal{E}_I$. The energy units will be effective Ry and

TABLE III. Parabolic coordinate eigenfunctions in terms of spherical coordinate eigenfunctions for hydrogen atom in the limit of $\mathcal{E} \to 0$. The $m \neq 0$ states are not included, because they do not contribute to the direct exciton spectrum.

ϕ_{nim}	ϕ_{nlm}
$\phi_{110} =$	$R_{10}Y_{00}$
$\phi_{210} =$	$\sqrt{\tfrac{1}{2}}R_{20}Y_{00} + \sqrt{\tfrac{1}{2}}R_{21}Y_{10}$
$\phi_{220} =$	$\sqrt{\tfrac{1}{2}}R_{20}Y_{00} - \sqrt{\tfrac{1}{2}}R_{21}Y_{10}$
$\phi_{310} =$	$\sqrt{\tfrac{1}{3}}R_{30}Y_{00} + \sqrt{\tfrac{1}{2}}R_{31}Y_{10} + \sqrt{\tfrac{1}{6}}R_{32}Y_{20}$
$\phi_{320} =$	$\sqrt{\tfrac{1}{3}}R_{30}Y_{00} - \sqrt{\tfrac{2}{3}}R_{32}Y_{20}$
$\phi_{330} =$	$\sqrt{\tfrac{1}{3}}R_{30}Y_{00} - \sqrt{\tfrac{1}{2}}R_{31}Y_{10} + \sqrt{\tfrac{1}{6}}R_{32}Y_{20}$

$\phi^2(0)$ will be normalized such that it approaches $(E - E_g)^{1/2}$ for $E \gg E_g$. This is in accordance with Elliott's continuum density of states for optical absorption by excitons. He calculated that for zero electric field[3]

$$\phi^2(0) = 2\pi/[1 - \exp(-2\pi E_d^{-1/2})], \quad E > E_g \quad (61)$$

where

$$E_d = E - E_g \text{ and } \phi^2(0) \to (E - E_g)^{1/2} \text{ for } E \gg E_g.$$

Elliott also calculated that the zero-field intensity of the bound exciton lines $(E < E_g)$ was given by $4\pi n^3$ and

$$\phi^2(0) = \sum_{n=1}^{\infty} 4\pi n^{-3} \delta(E - E_g + n^{-2}), \quad E < E_g. \quad (62)$$

For $n \to \infty$, it may be shown that $\phi^2(0)$ approaches the continuum value of 2π. It will be shown in what way the electric field alters the zero-field spectrum as described by Eqs. (61) and (62). Equations (61) and (62) do not include the possibility of line broadening which must be included if a valid comparison between theory and experiment is to be made. Broadening will be included in a subsequent paper[29] so that experiment and theory may be compared.

In Fig. 7, the exciton spectrum is shown for four different values of $F = \mathcal{E}/\mathcal{E}_I$. For $F = 0.005$, it is evident that the electric field has had little effect on the $1s$ or $2s$ hydrogenic levels. The $n = 3$ and higher levels are however greatly affected by this magnitude of electric field. The $n = 3$ level is split into three parts by this field and all higher levels are smeared into a continuum. The three Stark-split branches of the $n = 3$ level correspond to mixtures of the $3s$, $3p$, and $3d$ hydrogenic states for small F. States with zero s character have been omitted. In terms of the $R_{nl}Y_{lm}$ hydrogenic wave functions, the three branches correspond to

$$\phi(n=3) = \begin{cases} \sqrt{\tfrac{1}{3}}R_{30}Y_{00} + \sqrt{\tfrac{1}{2}}R_{31}Y_{10} + \sqrt{\tfrac{1}{6}}R_{32}Y_{20} & \text{(lower branch)} \\ \sqrt{\tfrac{1}{3}}R_{30}Y_{00} - \sqrt{\tfrac{2}{3}}R_{32}Y_{20} & \text{(middle branch)} \\ \sqrt{\tfrac{1}{3}}R_{30}Y_{00} - \sqrt{\tfrac{1}{2}}R_{31}Y_{10} + \sqrt{\tfrac{1}{6}}R_{32}Y_{20} & \text{(upper branch).} \end{cases} \quad (63)$$

One very interesting effect of this splitting is that the lower branch which presumably lies deepest in the well is the one most broadened by the electric field. This broadening is a result of the spacial distribution of the wave functions in the well. If the wave function is more concentrated on the lip side of the well then the chances of the electron escaping from the hole are improved and the probability $\phi^2(0)$ is reduced. This is exactly the case here. The $\phi^2(0)$ for the lower branch is broader because the wave function is concentrated on the lip

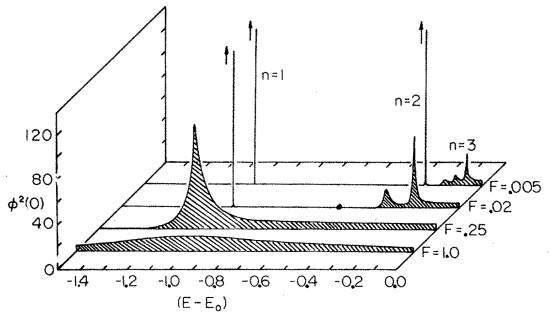

FIG. 7. Electric field effect on bound exciton levels for $F=\mathcal{E}/\mathcal{E}_I=0.005$, 0.02, 0.25, and 1.0. The bound states are split and subsequently mixed into a continuum as the electric field lowers the lip of the Coulombic well.

side of the well and that level is more susceptible to ionization. This affect has been observed in the Stark effect on hydrogen.[15] Increasing F from 0.005 to 0.02 smears the $n=3$ levels into the continuum and splits the $n=2$ level into two parts. The two Stark-split branches of the $n=2$ level correspond to mixtures of $2s$ and $2p$ hydrogenic states for small F. In terms of the $R_{nl}Y_{lm}$ the two branches are given by

$$\phi(n=2)=\begin{cases}\sqrt{\frac{1}{2}}R_{20}Y_{00}+\sqrt{\frac{1}{2}}R_{21}Y_{10} & \text{(lower branch)}\\ \sqrt{\frac{1}{2}}R_{21}Y_{00}-\sqrt{\frac{1}{2}}R_{21}Y_{10} & \text{(upper branch).}\end{cases} \tag{64}$$

Again the lowest energy branch has been broadened the most by the electric field which is due to the fact that its wave function has a higher probability on the lip side of the well and thus a greater chance to escape. Increasing F from 0.02 to 0.25 smears the $n=2$ levels into the continuum and broadens and shifts the $n=1$ exciton level. The $n=1$ level corresponds to the $1s$ hydrogenic state, which is given by

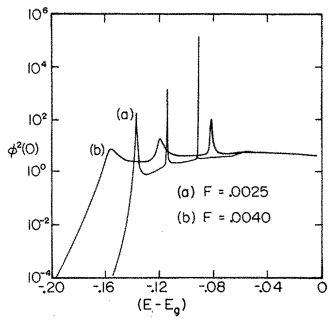

FIG. 8. Electric field effect on $n=3$ hydrogenic level for $F=\mathcal{E}/\mathcal{E}_I=0.0025$ and 0.0040.

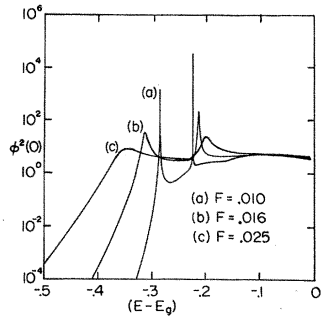

FIG. 9. Electric field effect on $n=2$ hydrogenic level for $F=\mathcal{E}/\mathcal{E}_I=0.010$, 0.016, and 0.025.

$$\phi(n=1)=R_{10}Y_{00}. \tag{65}$$

This ground state of the exciton shows the quadratic Stark shift to lower energies for $F<0.5$ and at $F\simeq 0.7$ starts shifting back to higher energies due to mixing with the continuum. For $F\geq 1.0$, no bound exciton levels are distinguishable and the electric field has completely ionized the exciton.

In Figs. 8–10 the effect of a uniform electric field on transitions to the first three bound exciton levels is seen in more detail. Figure 8 omits the $n=1$ and $n=2$ levels and shows the Stark splittings, shifts, and broadening of the $n=3$ level for $F=0.0025$ and 0.0040. Again it is interesting to note that the lower branch is shifted and broadened more extensively than the higher two branches of the $n=3$ level. Figure 9 omits the $n-1$ level and shows the Stark splittings, shifts, and broadening of the $n=2$ level for $F=0.010$, 0.016, and 0.025. Figure 10 shows the Stark shift and broadening of the $n=1$ level for $F=0.10$, 0.32, and 1.0. These shifts agree quite well with the energies as calculated from perturbation theory as given by Eq. (60) for $F<0.5$. But for $F>0.5$, the perturbative result differs from the actual result as the hydrogenic set of wave functions cannot describe the continuum

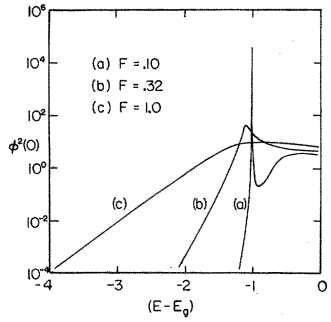

FIG. 10. Electric field effect on $n=1$ hydrogenic level for $F=\mathcal{E}/\mathcal{E}_I=0.10$, 0.32, and 1.0.

spectrum resulting from the application of the electric field.

D. Continuum States

For $F>1$, $\phi^2(0)$ approaches the limit in which the electric field completely dominates the Coulomb field. In fact, for $F>10$ there is very little difference between the $\phi^2(0)$ calculated including Coulomb potential and $\phi^2(0)$ calculated excluding the Coulomb potential. For electric fields $F>1$, absorption by the bound exciton states no longer dominates the spectrum, and the continuum exciton states become important. Since Eq. (31) for $\phi_n(\vec{r})$ does not specify whether the reduced mass μ of the electron-hole pair be positive or negative, it is possible to use Eq. (31) to calculate the electric field plus Coulomb field effects near both M_0(positive μ) and M_3 (negative μ) type critical points in the energy band structure. Critical points in the energy band structure are points in $\vec{k}$ space where the conduction and valence bands are parallel. At a critical point $\nabla_{\vec{k}}(E_c-E_v)=0$ which causes a singularity in the interband density of states which may be expressed as

$$\rho(E_{cv})=\frac{2}{(2\pi)^3}\int\frac{dS}{|\nabla_{\vec{k}}E_{cv}(\vec{k})|}\quad, \tag{66}$$

where S is a surface of constant interband energy $E_{cv}(\vec{k})$. Equation (66) does not include the electron-hole interaction or the electric field and is thereby inadequate for our purposes, but it does demonstrate which regions of $\vec{k}$ space are important in terms of causing structure in the interband density of states. In the immediate vicinity of a critical point $\vec{k}_0$ in the Brillouin zone, the energy $E(\vec{k})$ is a quadratic function of the directional components of $\vec{k}-\vec{k}_0$, namely, $\Delta k_\alpha=(\vec{k}-\vec{k}_0)_\alpha$:

$$E(\vec{k})=E(\vec{k}_0)+\tfrac{1}{2}\hbar^2\left(\frac{\Delta k_1^2}{\mu_1}+\frac{\Delta k_2^2}{\mu_2}+\frac{\Delta k_3^2}{\mu_3}\right), \tag{67}$$

where the μ_α are defined as

$$\mu_\alpha^{-1}=m_{e\alpha}^{*-1}+m_{h\alpha}^{*-1}, \tag{68}$$

where $m_{e\alpha}$ and $m_{h\alpha}$ are the effective masses for the electron and hole along the α direction. There are four types of critical points M_0, M_1, M_2, and M_3 which may be defined as[38]

$M_0\equiv\mu_1,\mu_2,\mu_3$ all positive;

$M_1\equiv\mu_1,\mu_2$ positive, μ_3 negative;

$M_2\equiv\mu_1,\mu_2$ negative, μ_3 positive;

$M_3\equiv\mu_1,\mu_2,\mu_3$ all negative.

The number of critical points for transitions between two bands depends on each individual band structure, but the minimum number of critical points is fixed by the number of nondegenerate high-symmetry points in the Brillouin zone.[39]

In our case where both the Coulomb potential and electric field are included, it was necessary to assume an isotropic mass to make the problem soluble. Thus we are limited to the case where μ_1, μ_2, and μ_3 are all equal and have the same sign. The M_0 (positive μ) and M_3 (negative μ) critical points are referred to as being absorption edges; the M_0 edge is the fundamental edge at the band gap and the M_3 edge corresponds to transitions from the bottom of the valence band to the top of the conduction band.

The use of parabolic coordinates gives a clear picture of the origin of the electric-field-induced oscillations in the continuum of $\phi^2(0)$, as demonstrated in Fig. 11 for $F=\mathcal{E}/\mathcal{E}_I=1$. As shown in Fig. 11, the total function $\phi^2(0)$ is a sum over individual functions $\phi_i^2(0)$ where

$$\phi_i^2(0)=(\mathcal{E}/\mathcal{E}_I)^{1/3}f_{\kappa_i}^2(0)g_{\kappa_i'}^2(0),\qquad \kappa_i'=\kappa_i+2(\mathcal{E}/\mathcal{E}_I)^{1/3}, \tag{69}$$

where these functions have been defined previously. Each function $\phi_i^2(0)$ contributes a bump in the spectra with the total result being an induced oscillation in the density of states. For high fields $\mathcal{E}/\mathcal{E}_I\gg1$, the bumps center on the β_i defined in Eq. (56) and

$$\phi_i^2(0)\sim\left(\frac{\mathcal{E}}{\mathcal{E}_i}\right)^{1/3}\left(\frac{\gamma_i}{(\beta-\beta_i)^2+\gamma_i^2}\right), \tag{70}$$

where γ_i decreases slowly with increasing i. For large β ($E\gg E_g$) it may be demonstrated that $\phi^2(0)=\sum_i\phi_i^2(0)$ approaches the desired limit $[(E-E_g)/R]^{1/2}$ using the $\phi_i^2(0)$ as defined in Eq. (70).[40]

Figure 12 shows $\phi^2(0)$ near an M_0-type edge for $F=1$, 10, and 100. For $F=1$, a small exciton peak below the edge is still in evidence. If a comparison were made between the calculated values of the amplitude of the oscillations in $\phi^2(0)$ above the edge

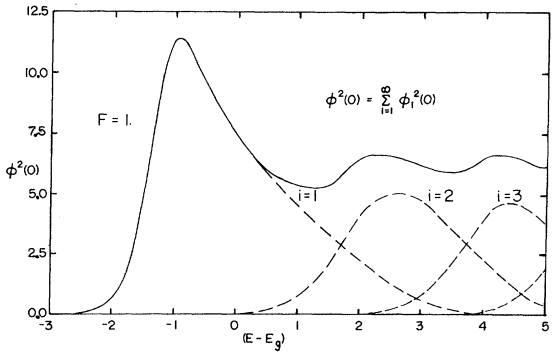

FIG. 11. Contributions of individual amplitudes $\phi_i^2(0)$ for $F=\mathcal{E}/\mathcal{E}_I=1$. Each eigenvalue contributes one bump to the continuum for $\mathcal{E}\geq\mathcal{E}_I$ and in the limit $\mathcal{E}\gg\mathcal{E}_I$, these bumps are centered on $(E-E_g)\sim(\mathcal{E}/\mathcal{E}_I)^{2/3}\beta_i$, where $\beta_i=[(\frac{3}{2}\pi i-\frac{1}{2})]^{2/3}$.

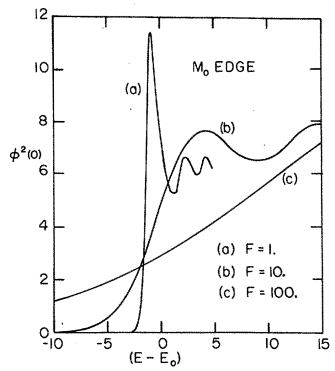

FIG. 12. Field dependence of optical absorption near an M_0-type edge for $F = \mathcal{E}/\mathcal{E}_I = 1.0$, 10.0, and 100.0.

with and without the electron-hole interaction, it would be quite evident that the Coulomb potential enhances the electric-field-induced oscillations above the edge as well as causing absorption peaks below the edge. Thus, even if the electric field is strong enough to ionize the bound exciton levels, the Coulomb potential still contributes through the amplitude of the electric-field-induced oscillations above the edge. For $F = 10$ and 100, the oscillations spread out approximately as $F^{2/3}$ and no peaks below the edge are noticeable.

Figure 13 shows $\phi^2(0)$ near an M_3-type edge for $F = 1$, 10, and 100. Having a negative mass and an attractive Coulomb potential is the same thing mathematically as having a positive mass and a repulsive Coulomb potential. Thus we would expect that inclusion of the electron-hole interaction would decrease $\phi^2(0)$ near an M_3-type edge. This is to say that if $\phi^2(0)$ is the probability of an electron and hole being at the same point in the crystal then inclusion of a repulsive electron-hole interaction should reduce $\phi^2(0)$. This is exactly what happens. The repulsive Coulomb potential not only reduces the magnitude of $\phi^2(0)$ but it also reduces the amplitude of the electric-field-induced oscillations near an M_3-type edge. This is perhaps one reason why M_3 edges have not been observed in electroreflectance, i.e., the optical density of states is actually changing so slowly near an M_3-type edge that electric-field-induced changes are insignificant.

IV. DISCUSSION

The theoretical results contained within this paper require several assumptions: (a) The excitation spans several unit cells of the crystal; (b) the conduction and valence bands are isotropic near the band edge and have constant curvature; (c) the electric field is uniform; (d) the optical transitions are direct (vertical in $\vec{k}$ space) and allowed; and (e) the effective charges on the electron and hole are screened by the static dielectric constant. All of these assumptions allow the problem of the Wannier exciton in an electric field to be reduced to the problem of a hydrogenlike atom in a uniform electric field. The Schrödinger equation for the hydrogenic atom in a uniform electric field is separable in parabolic coordinates thereby allowing the equation to be solved numerically. In parabolic coordinates, the eigenvalues are an azimuthal quantum number m, a separation constant ν, and energy E. For finite electric fields, energy is a continuous eigenvalue and normalization to a Dirac δ function instead of a Kronecker δ is required. A normalization procedure for continuous eigenvalues is outlined in Sec. III B showing that the coefficient of the oscillatory asymptotic solution determines the proper normalization for the energy eigenvalue.

The connection between physical parameters, such as the absorption coefficient α or the imaginary part of the dielectric constant ϵ_2, and the calculated wave functions was demonstrated in Sec. II and the first part of Sec. III. The absorption coefficient α and the imaginary part of the dielectric constant ϵ_2 are related by

$$\epsilon_2 = (nc/\omega)\alpha \ , \tag{71}$$

where n is the index of refraction of the solid, c is the speed of light in vacuum, and $\omega = 2\pi\nu$, where ν is the frequency of the electromagnetic wave. By Eq. (30) near the direct edge, ϵ_2 is also given by

$$\epsilon_2 = \tfrac{4}{3}\epsilon \ |(\vec{\mu}_{cv}/ea)|^2 \phi^2(0) \ , \tag{72}$$

where ϵ is the static dielectric constant, $\vec{\mu}_{cv}$ is an interband dipole matrix element defined by Eq.

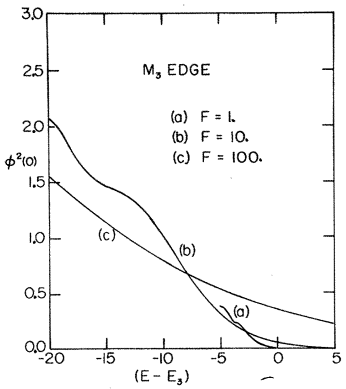

FIG. 13. Field dependence of optical absorption near an M_3-type edge for $F = \mathcal{E}/\mathcal{E}_I = 1.0$, 10.0, and 100.0, By comparison of the M_0 and M_3 edges, it is evident that the electron-hole interaction enhances the electric-field-induced oscillations near an M_0 edge (positive effective masses) and quenches these oscillations near an M_3 edge (negative effective masses).

(29), e is the electronic charge, a is the exciton radius, and $\phi^2(0)$ is a density-of-states function normalized to approach

$$\phi^2(0) \sim [(\hbar\omega - E_g)/R]^{1/2}, \quad (\hbar\omega - E_g) \gg R \tag{73}$$

where E_g is the direct energy gap and R is the exciton binding energy. From Eq. (72), it is evident that the oscillator strength of the interband transition enters only as a prefactor to the density-of-states function $\phi^2(0)$ along with the size of the excitation. The exciton radius a is given by Eq. (3) and increases linearly with increasing dielectric constant for constant effective mass. In most cases, higher dielectric constants imply more mobile carriers and smaller effective masses, thus the radius a should increase at a greater rate than linearly with increasing dielectric constant which would cause the exciton absorptive strength to be proportional to ϵ^{-b} where $b \geq 1$.

The density-of-states function $\phi^2(0)$ contains all the excitonic structure and all electric field effects. The wave function $\phi_n(\vec{r})$ is the solution to the hydrogenic Schrödinger equation for the state n with energy E_n and is related to $\phi^2(0)$ by Eq. (26),

$$\phi^2(0) = 4\pi^2 a^3 \textstyle\sum_n |\phi_n(0)|^2 \delta[(E_g + E_n - \hbar\omega)/R] \ , \tag{74}$$

which for zero field $\vec{\mathcal{E}} = 0$ reduces to Eqs. (27),

$$\phi^2(0) = 4\pi \sum_{n=1}^{\infty} n^{-3} \delta\left[\frac{(\hbar\omega - E_g + Rn^{-2})}{R}\right], \quad \hbar\omega < E_g \tag{75a}$$

$$\phi^2(0) = 2\pi \Big/ \left\{1 - \exp\left[-2\pi\left(\frac{\hbar\omega - E_g}{R}\right)^{-1/2}\right]\right\}, \quad \hbar\omega > E_g . \tag{75b}$$

Equation (75a) exhibits the hydrogenic series with absorptive strengths proportional to n^{-3} and Eq. (75b) exhibits the continuum above the edge and has the desired limiting form of Eq. (73). Both Eqs. (75a) and (75b) approach the limit of $\phi^2(0) = 2\pi$ for $\hbar\omega = E_g$, below the edge as a quasicontinuum,

$$\phi^2(0) \sim 4\pi n^{-3} R \left(\frac{\partial E_n}{\partial n}\right)^{-1},$$

and as a continuum above the edge.

The solution to the hydrogenic Schrödinger equation for finite electric field is discussed in detail in Secs. III A and III B. This solution requires separation in parabolic coordinates and normalization for a continuous energy eigenvalue as discussed previously. With appropriate definition of dimensionless variables, the solution requires evaluating two functions $f_\kappa(x)$ for $x > 0$ and $g_{\kappa'}(x)$ for $x < 0$ where κ, κ', and x are defined by Eqs. (39) and (40). The solutions of the equation for $f_\kappa(x)$ determine eigenvalues κ_i, $i = 1, 2, 3, 4, \ldots$, which are continuous functions of energy. The expression for $\phi^2(0)$ in terms of these parabolic coordinate eigenfunctions f and g is, at every energy, given by

$$\phi^2(0) = \left(\frac{\mathcal{E}}{\mathcal{E}_I}\right)^{1/3} \sum_{i=1}^{\infty} f^2_{\kappa_i}(0) g^2_{\kappa_i'}(0) \ , \tag{76a}$$

$$\kappa_i' = \kappa_i + 2(\mathcal{E}/\mathcal{E}_I)^{-1/3}. \tag{76b}$$

The amplitude $f^2_{\kappa_i}(0)$ is a slowly varying function of energy, but falls off quickly for $\kappa_i > 0$. The zeroes of the κ_i are dependent on the field $\mathcal{E}$ and are given by $\kappa_i(E_i) = 0$, where E_i is approximated by

$$E_i = E_g + R(\mathcal{E}/\mathcal{E}_I)^{2/3}\beta_i \ , \tag{77a}$$

$$\beta_i = [\tfrac{3}{2}\pi(i - \tfrac{1}{2})]^{2/3}, \quad i = 1, 2, 3, 4, \ldots \ . \tag{77b}$$

Thus for $E > E_i$ the amplitude $f^2_{\kappa_i}(0)$ falls off rapidly. Below the edge,

$$f^2_{\kappa_i}(0) \sim (\mathcal{E}/\mathcal{E}_I)^{-1/3}[(E_g - \hbar\omega)/R]^{1/2} \ .$$

The excitonic peaks are contained in $g^2_{\kappa_i'}(0)$ as demonstrated in Secs. III B and III C.

The degree that a bound state is affected by the electric field and the type of effect are dependent on two factors: (a) the depth of the level in the well and (b) the spacial distribution of the wave function in the well. The importance of the first factor is obvious as it is simply a measure of the binding energy of the level; but the importance of the second factor is not so obvious and is due to the asymmetry of the electric field potential. For instance, since the electric field lowers only one side of the Coulombic well as shown in Fig. 1, an electron which spends more time on the lip side has a greater probability of escaping. This is evident from the different broadenings of the two split-off branches of the $n = 2$ hydrogenic level as shown in Fig. 9. The lower-energy branch is broadened more extensively by the electric field because it has a higher probability of being on the lip side of the well. A second-order effect of the electric field is to slightly widen the well which causes the symmetric $n = 1$ hydrogenic level to move down in the well. As the electric field increases, the lip of the well passes one bound level after another until for $\mathcal{E} > \mathcal{E}_1$ all bound levels are mixed into a continuum as shown in Fig. 7.

For $\mathcal{E} < \mathcal{E}_I$, the exciton lines dominate the spectra, but, for $\mathcal{E} > \mathcal{E}_I$, the electric-field-induced oscillations in the continuum are of primary interest. These oscillations have been calculated in the no electron-hole interaction limit,[41] but the effect of the electron-hole interaction on these oscillations has not been demonstrated before. There are two cases treated in Sec. III D: (a) for an M_0-type edge (positive effective masses) and (b) for an M_3-type edge (negative effective masses). The unequivocal result is that the electron-hole interaction enhances the electric-field-induced oscillations near an M_0-

type edge and quenches these oscillations near an M_3-type edge. This result may explain the fact that M_3-type edges have not been observed in electroreflectance.

In summary, this paper presents a comprehensive study of electric field effects on optical absorption by the hydrogenlike Wannier exciton. The field effects on both bound and continuum states are presented. The calculations and results have been simplified by defining appropriate dimensionless parameters. A general normalization procedure for wave functions with continuous eigenvalues is outlined. The effect of the electron-hole interaction on the electric-field-induced oscillations is demonstrated for the first time. Some related problems that are still outstanding are: (a) field effects on forbidden transitions, as in Cu_2O,[42,43] (b) inhomogeneous field effects in excitonic electroabsorption,[44] and (c) excitonic electroabsorption near M_1 and M_2 critical points, where the masses not only are anisotropic, but are either positive or negative depending on direction. Excitonic electroabsorption will be presented and compared with experiment in a subsequent paper.[29]

ACKNOWLEDGMENTS

I would like to express thanks to Professor Paul Handler for guidance throughout this investigation and to Dr. D. E. Aspnes and Dr. J. D. Dow for valuable comments. I would also like to thank Mrs. Nancy A. Kaiser for careful typing of the manuscript.

APPENDIX: WKB EIGENVALUES

The differential equation that determines the eigenvalues $\kappa_i(\beta)$ is given by Eq. (43):

$$\frac{1}{x}\frac{d}{dx}\left(x\frac{df}{dx}\right)+\left(\frac{-\kappa}{x}+\beta-x\right)f=0, \quad 0\le x\ . \tag{A1}$$

In the WKB approximation, it is possible to calculate these eigenvalues by requiring that the change in phase of the wave function between classical turning points be given by

$$\int_{x_1}^{x_2} dx(-\kappa_i/x+\beta-x)^{1/2}=(i-\tfrac{1}{2})\pi, \quad i=1,2,3,4,\ldots \tag{A2}$$

where x_1 and x_2 are the classical turning points. As it turns out these values κ_i^{WKB} are very good starting points for calculating the $\kappa_i(\beta)$ numerically. All of the κ_i^{WKB} were well within 1% of the actual eigenvalues. Calculation of the WKB eigenvalues may be divided into three parts: $\kappa<0$, $\kappa=0$, and $\kappa>0$.

Let us define the parameters A and B as

$$A=\tfrac{1}{2}[\beta-(\beta^2-4\kappa)^{1/2}]\ , \tag{A3a}$$

$$B=\tfrac{1}{2}[\beta+(\beta^2-4\kappa)^{1/2}] \tag{A3b}$$

and calculate the integral in Eqs. (A3).

$\kappa<0$

For $\kappa<0$ the classical turning points are $x_1=0$, $x_2=B$, thus

$$(i-\tfrac{1}{2})\pi=\int_0^B dx\left(\frac{(x-A)(B-x)}{x}\right)^{1/2}$$
$$=B(B-A)^{1/2}B(\tfrac{3}{2},\ \tfrac{1}{2})F(-\tfrac{1}{2},\ \tfrac{3}{2};\ 2;\ Z), \tag{A4}$$

where B is the β function, F is a hypergeometric function and $Z=B/(B-A)$. If we define a set of functions

$$f_i=(i-\tfrac{1}{2})\pi B^{-1}(B-A)^{-1/2} \tag{A5}$$

then these may be plotted versus

$$F_a=B(\tfrac{3}{2},\ \tfrac{1}{2})F(-\tfrac{1}{2},\ \tfrac{3}{2};\ 2;\ Z)$$

to achieve a graphical solution of Eq. (81) as shown in Fig. 14(a).

$\kappa=0$

The solution of Eqs. (A3) for $\kappa_i=0$ is given as

$$(i-\tfrac{1}{2})\pi=\tfrac{2}{3}\beta_i^{3/2}\ . \tag{A6}$$

Thus the zeros of the κ_i^{WKB} occur at

$$\beta_i=[\tfrac{3}{2}\pi(i-\tfrac{1}{2})]^{2/3}\ . \tag{A7}$$

$\kappa>0$

For $\kappa>0$ the classical turning points are $x_1=A$ and $x_2=B$, thus

$$(i-\tfrac{1}{2})\pi=\int_A^B dx\left(\frac{(x-A)(B-x)}{x}\right)^{1/2}$$

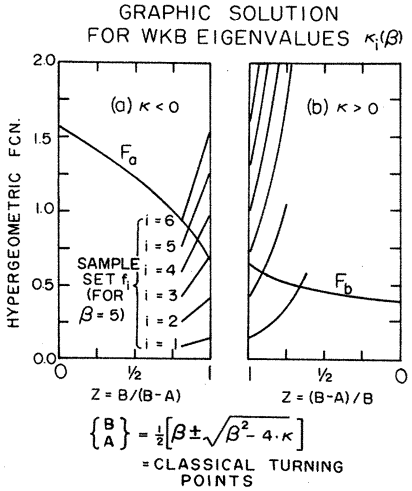

FIG. 14. Graphical solution for WKB eigenvalues κ_i^{WKB}.

$$= (B-A)^2 B^{-1/2} B(\tfrac{3}{2}, \tfrac{3}{2}) F(\tfrac{1}{2}, \tfrac{3}{2}; 3; Z), \qquad \text{(A8)}$$

where $Z = (B-A)/B$. If we again define a set of functions f_i as

$$f_i = (i - \tfrac{1}{2})\,\pi B^{1/2}(B-A)^{-2}, \qquad \text{(A9)}$$

then Eq. (A9) may be solved graphically by plotting f_i versus $F_b = B(\tfrac{3}{2}, \tfrac{3}{2}) F(\tfrac{1}{2}, \tfrac{3}{2}; 3; Z)$ as shown in Fig. 14(b).

---

*Work supported in part by the U. S. Army Research Office, Durham, N. C.

†NASA Fellow, present address: Xerox Research Laboratories, Xerox Square, Rochester, N. Y. 14603.

[1]G. H. Wannier, Phys. Rev. 52, 191 (1937).

[2]G. Dresselhaus, J. Phys. Chem. Solids 1, 14 (1956).

[3]R. J. Elliott, Phys. Rev. 108, 1384 (1957).

[4]R. J. Elliott, in *Polarons and Excitons*, edited by C. G. Kuper and G. D. Whitfield (Oliver and Boyd, Edinburgh, 1963), p. 269ff.

[5]J. Frenkel, Phys. Rev. 37, 17 (1931).

[6]J. Frenkel, Phys. Rev. 37, 1276 (1931).

[7]R. E. Peierls, Ann. Physik 13, 905 (1932).

[8]A. W. Overhauser, Phys. Rev. 101, 1702 (1956).

[9]R. S. Knox, in *Solid State Physics*, edited by F. Seitz and D. Turnbull (Academic, New York, 1963), Suppl. 5.

[10]J. O. Dimmock, in *Semiconductors and Semimetals*, edited by R. K. Willardson and A. C. Beer (Academic, New York, 1966), Vol. 3, p. 259ff.

[11]R. A. Smith, *Semiconductors* (Cambridge U. P., Cambridge, England, 1961), pp. 347, 350, 367, and 410.

[12]C. Hilsum, in *Semiconductors and Semimetals*, edited by R. K. Willardson and A. C. Beer (Academic, New York, 1966), Vol. 1, p. 9.

[13]Reference 10, p. 314.

[14]O. Madelung, *Physics of III–V Compounds* (Wiley, New York, 1964), p. 101.

[15]B. Segall and D. T. F. Marple, in *Physics and Chemistry of II-VI Compounds*, edited by M. Aven and J. S. Prener (Wiley, New York, 1967), pp. 335 and 344.

[16]C. Lanczos, Z. Physik 62, 518 (1930); 68, 204 (1931).

[17]H. Rausch von Traubenberg and R. Gebauer, Z. Physik 54, 307 (1929); 56, 254 (1929); 62, 289 (1930); 71, 291 (1931).

[18]J. R. Oppenheimer, Phys. Rev. 31, 66 (1928).

[19]H. A. Bethe and E. E. Salpeter, *Quantum Mechanics of One and Two-Electron Atoms* (Academic, New York, 1957).

[20]C. B. Duke and M. E. Alferieff, Phys. Rev. 145, 583 (1966).

[21]H. I. Ralph, J. Phys. C 1, 378 (1968).

[22]J. D. Dow and D. Redfield, Phys. Rev. B 1, 3358 (1970).

[23]D. F. Blossey, Bull. Am. Phys. Soc. 14, 429 (1969).

[24]D. F. Blossey, Ph. D. thesis, University of Illinois, 1969 (unpublished).

[25]F. Urbach, Phys. Rev. 92, 1324 (1953).

[26]R. Enderlein, Phys. Status Solidi 26, 509 (1986).

[27]J. D. Dow, Phys. Status Solidi 34, K71 (1969).

[28]C. M. Penchina, J. K. Pribram, and J. Sak, Phys. Rev. 188, 1240 (1969).

[29]D. F. Blossey (unpublished). The term electroabsorption as it is used here refers to the electric-field-modulated spectrum which is the difference between the finite- and zero-field spectra.

[30]M. Cardona, in *Solid State Physics*, edited by F. Seitz, D. Turnbull, and H. Ehrenreich (Academic, New York, 1969), Suppl. 11; V. O. Seraphin, in *Semiconductors and Semimetals*, edited by R. K. Willardson and A. C. Beer (Academic, New York, 1970), Vol. 6; D. E. Aspnes and N. Bottka, *ibid.*; D. F. Blossey and P. Handler, *ibid.*, Vol. 9.

[31]J. Hermanson, Phys. Rev. Letters 18, 170 (1967).

[32]C. M. Penchina, Phys. Rev. 130, 2204 (1963).

[33]L. Fritsche, Phys. Status Solidi 11, 381 (1965).

[34]M. Chester and L. Fritsche, Phys. Rev. 139, A518 (1965).

[35]Y. Yacoby, Phys. Rev. 140, A263 (1965).

[36]W. S. Chow, Phys. Rev. 185, 1056 (1969); 185, 1062 (1969).

[37]I. S. Grandshteyn and I. M. Ryzhik, *Table of Integrals, Series, and Products* (Academic, New York, 1965), p. 1040ff.

[39]L. VanHove, Phys. Rev. 89, 1189 (1953); J. C. Phillips, *ibid.* 104, 1263 (1956); J. C. Phillips, in *Solid State Physics*, edited by F. Seitz and D. Turnbull (Academic, New York, 1966) Vol. 18, p. 55ff.

[38]D. Brust, J. C. Phillips, and F. Bassani, Phys. Rev. Letters 9, 94 (1962); D. Brust, Phys. Rev. 134, A1337 (1964).

[40]The density-of-states function $\phi^2(0)$ may be expressed as a sum over the $\phi_i^2(0)$ where the index i refers to the eigenvalue κ_i, $i = 1, 2, 3, 4, \ldots$. In the limit of $\mathcal{E} \gg \mathcal{E}_I$, the $\phi_i^2(0)$ each contribute one peak to the continuum spectra centered about $(E - E_g)/R = (\mathcal{E}/\mathcal{E}_I)^{2/3}\beta_i$, where $\beta_i = [(\frac{3}{2}\pi i - \frac{1}{2})]^{2/3}$ and the β_i are the zeros of the $\kappa_i(\beta)$. Far above the edge $E \gg E_g$, the $\phi_i^2(0)$ form a quasicontinuum limit in which $\phi^2(0) \sim (\mathcal{E}/\mathcal{E}_I)^{1/3}\pi(\partial\beta_i/\partial i) = [(E - E_g)/R]^{1/2}$ which is the desired limit. It should be emphasized that Eq. (70) is an empirical expression, and is only used to emphasize the fact that each electric-field-induced oscillation is due to a different parabolic-coordinate eigenvalue.

[41]D. E. Aspnes, Phys. Rev. 147, 554 (1966); 153, 972 (1967); D. E. Aspnes, Paul Handler, and D. F. Blossey, *ibid.* 166, 921 (1968).

[42]M. Grossmann, in *Polarons and Excitons*, edited by C. G. Kuper and G. D. Whitfield (Oliver and Boyd, Edinburgh, 1963), p. 374ff.

[43]S. Brahms and M. Cardona, Solid State Commun. 6, 733 (1968).

[44]D. E. Aspnes and A. Frova, Solid State Commun. 7, 155 (1969).